

Theoretical analysis and predictive modelling of ELMs mitigation by enhanced toroidal ripple and ergodic magnetic field

V. Parail¹, T. Evans², T. Johnson³, J. Lonnroth⁴, N. Oyama⁵, G. Saibene⁶, R. Sartori⁶, A. Salmi⁴, P. de Vries¹, M. Becoulet⁷, G. Corrigan¹, J. Hastie¹, C. Gimblett¹, C.M. Greenfield², T. Hatae⁵, D. Howell¹, V. Hynönen⁴, Y. Kamada⁵, T. Kiviniemi⁴, T. Kurki-Suonio⁴, A. Loarte⁶, E. Nardon⁷, K. Shinohara⁵ and JET EFDA contributors^{a)}

¹ EURATOM/UKAEA Fusion Association, Culham Science Centre, Abingdon OX14 3DB, United Kingdom;

² General Atomics, P.O. Box 85608, San Diego, California USA;

³ Association EURATOM-VR, Alfvén Laboratory, Royal Institute of Technology, 10044 Stockholm, Sweden;

⁴ Association EURATOM-TEKES, Helsinki University of Technology, P.O. Box 2200, FIN-02015 HUT, Finland;

⁵ Japan Atomic Energy Agency, Naka, Ibaraki-ken, 311-0193, Japan;

⁶ EFDA CSU – Garching, D85748 Garching, Germany;

⁷ Association Euratom-CEA, Cadarache 13108 Saint Paul LEZ DURANCE, FRANCE;

e-mail contact of main author: vparail@jet.uk

Abstract. Ripple-induced transport and externally driven resonance magnetic perturbations (RMP) near the separatrix are considered as prospective methods of ELM mitigation in present day tokamaks and ITER. Although these methods rely on different physics to generate extra transport, the influence of this transport on plasma dynamics and ELM mitigation is either similar or supplementary. The results of extensive theoretical analysis of the underlying physics processes behind transport induced by ripple and RMP is presented together with predictive transport modelling. Comparison with experiments on tokamaks is given.

I. Introduction.

The effects of ripple-induced losses on the performance of ELMy H-mode plasmas have been found in a number of experiments [1-3]. A noticeable difference in plasma confinement, toroidal rotation, ELM frequency and amplitude between JET (with ripple amplitude $\delta \sim 0.1\%$) and JT-60U (with $\delta \sim 1\%$) was found in otherwise identical discharges [1]. JT-60U plasmas generally has somewhat lower density and edge pressure with more frequent and smaller ELMs. It was previously shown in JET experiments with enhanced ripple [2] that a gradual increase in the ripple amplitude first leads to a modest improvement in plasma confinement (and earlier transition to H mode). This is followed by the degradation of edge pedestal and eventually a back transition to the L-mode regime, if δ increases above a certain critical level. The relative high impact of ripple induced transport on H-mode plasma is attributed to its reliance on the edge transport barrier (ETB) as the main cause of improved confinement. Since transport in a narrow layer at the edge of H-mode plasma is reduced to a very low, neo-classical level, the effects of any additional edge transport can be easily discernible.

ELM suppression by an externally induced stochastic magnetic field, which was recently successfully demonstrated in DIII-D [4], is another prospective method, which relies on extra transport induced within the ETB. Unlike ripple, an ergodic magnetic field mainly increases electron transport. However, both magnetic ripple and ergodic magnetic limiter tend to reduce plasma density. The physics of ELM suppression by both methods will be discussed in the paper with the results of theoretical analysis and predictive modelling compared with experiments.

II. ELM suppression by magnetic ripple.

The orbit following Monte Carlo code ASCOT was used to study the effect of toroidal ripple on the transport of thermal ions in JET and JT-60U magnetic configurations. Since JET has

^{a)} See Appendix of M.L. Watkins et al., *Fusion Energy 2006 (Proc. 21st Int. Conf. Chengdu, 2006) IAEA, Vienna (2006)*

32 toroidal field coils with a capability to change the ripple amplitude by varying the current in every second coil, we studied the dependence of ripple induced transport on ripple amplitude and configuration as well as on dimensionless plasma parameters like collisionality [5]. Two different techniques were used. The first method follows the drift orbits of test ions with a Maxwellian distribution, seeded in the whole plasma volume in accordance with

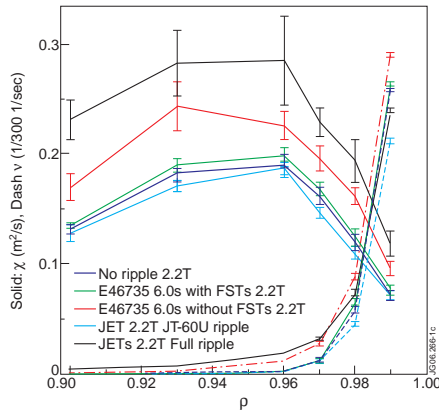


FIG. 1 Diffusive (solid) and convective (dashed) losses for JET plasmas with JET coils (maximum ripple-yellow, JT-60U ripple-pink, no ripple-long dashed) and JT-60U coils (without FST-red and with FST-green).

transport. It is also seen that the same level of magnetic ripple at the outer midplane generates more transport for the JT-60U magnetic configurations than for the JET one. This difference comes from the fact that JT-60U uses circular coils, which produce stronger ripple near the x-point than the D-shaped JET coils. ASCOT simulations also reveal that, depending on plasma collisionality, thermal ions can have both diffusive and convective losses. Diffusive losses are mainly associated with the ripple-banana diffusion [7], which gives a practically uniform toroidal distribution of lost particles and exhibits a wide region of enhanced transport, extending deep into the plasma core. On the other hand convective losses are mainly

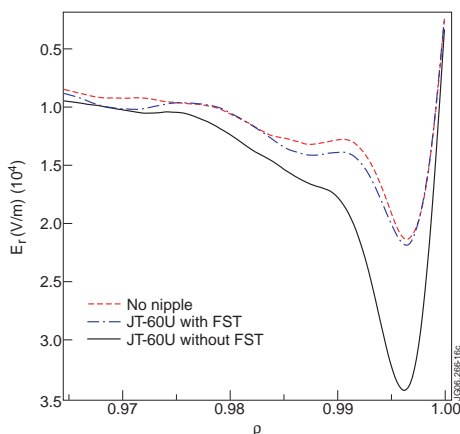


FIG. 2. Radial distribution of plasma electric field for JT-60U configuration without FST (black), with FST (blue) and without ripple (red).

attributed to the direct escape of locally trapped particles due to an uncompensated vertical drift. They are mainly present in low collisionality plasmas and are more visible in the JT-60U configuration because of the stronger ripple near the x-point, where the trajectory of an ion escaping due to vertical drift is much shorter than the trajectory of an ion escaping from the outer midplane.

ASCOT also allows calculation of the radial electric field distribution due to orbit losses, for varying level of B_T ripple. Figure 2 shows an example of such a distribution for the JT-60U configuration. We can conclude that ripple losses can significantly increase the radial electric field amplitude above the level, generated by the first orbit losses. It is worth noting that both the overall level of the radial electric field and its dependence on the ripple amplitude depend sensitively on the assumption of how strong is perpendicular ion viscosity, which balances the radial current induced by orbit and ripple losses. We conclude that JT-60U coils with FST do not generate extra electric field. This

translates into a reduction of toroidal rotation in counter-current direction, which indeed was recently reported by JT-60U [8].

The results of ASCOT simulation have been used as input to the predictive transport code JETTO, to simulate the dynamics of the ELMy H-mode JET plasmas in the presence of finite

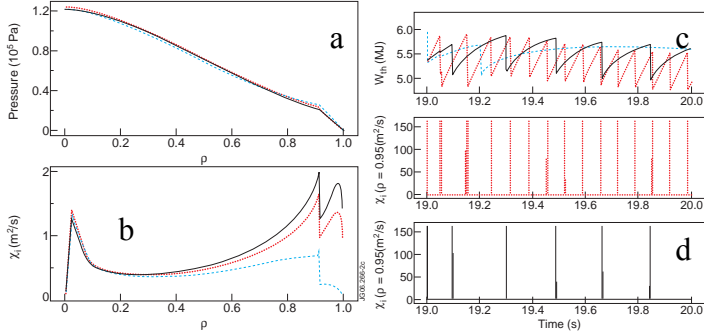


FIG. 3. Predictive transport modelling of JET plasma with the different level of wide ripple transport: red- without ripple, blue- medium ripple, pink- maximum ripple. a) plasma pressure just before ELM; b) ion thermal conductivity before ELM; c) time evolution of the energy content; d) ELM frequency for three level of convective losses.

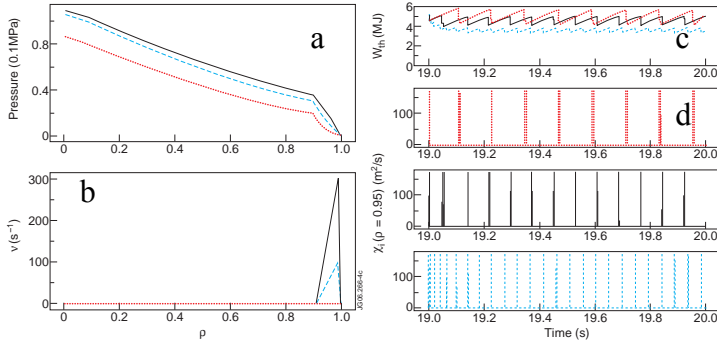


FIG. 4. Predictive modelling of JET plasma with edge-localized convective ripple losses. a) plasma pressure just before ELM for three different level of convective losses (red- without losses, blue- with moderate edge losses and pink- maximum losses). b) amplitude of convective losses; c) energy content and ELM frequency for three level of convective losses, d) ELM frequency.

ETB, leads to a significant decrease in ELM frequency, so that the energy and particle losses per ELM increase. This is accompanied by a slight increase in the energy content. The explanation for this effect comes from the recognition that energy confinement in ELMy H-mode depends on two ingredients. The first one is transport between ELMs and the other is transport during ELMs. By increasing transport between ELMs we can completely eliminate ELMs while keeping the plasma pressure at the top of the ETB very close to the maximum level permitted by the MHD stability. This increases the time-average top-of-barrier pressure, which translates into better confinement due to profile stiffness. This result is in line with earlier experimental observations from JET [2]. However, we should also take into account convective ripple losses due to the direct escape of locally trapped ions and those are very edge-localised. To take these convective losses into account we introduce a very simple ad

hoc model for convective ion losses: $\frac{\partial nT_i}{\partial t} = P + \text{div}q - \frac{nT_i}{\tau_{\text{ripple}}}$, where P is heating power,

ripple losses. The Bohm/gyroBohm model for anomalous transport was used together with the neo-classical transport within the ETB. A previously discussed model for ELMs was used [9], which triggers an ELM if the edge pressure gradient exceeds the critical level needed to destabilise ballooning or peeling modes. A simple analytical approximation for ripple-induced diffusive transport [7] was used, and its amplitude was adjusted using results of ASCOT simulations. Ripple amplitude scans show that this additional transport can have an impact on the severity of ELMs and overall plasma confinement. We first assume that ripple-induced transport has only a diffusive component, so that an increase of ion transport above the neo-classical level is almost uniform within the ETB (see Figure 3). This additional transport, in spite of being quite small with respect to anomalous transport inside the

$q = -\chi_i n_i \nabla T_i$ is the diffusive heat flux and τ_{ripple} is the characteristic edge confinement time, which decreases rapidly towards the separatrix due to convective ripple losses, see Figure 4. The result of predictive transport modelling is that convective transport might be a very effective tool for depleting the edge pedestal. Although convective transport does not eliminate ELMs, it reduces the ELM amplitude and increases the ELM frequency. This trend is accompanied by a noticeable degradation of plasma confinement, which initially comes from the flattening of the ion temperature near the separatrix due to highly localised ripple losses. Since the maximum pressure gradient is still limited by ballooning stability it effectively reduces the pressure at the top of the ETB (if pedestal width does not change). This reduction spreads all over the plasma core due to the stiffness of anomalous transport. It is important to note though that the main contribution to convective losses comes from the orbit losses, particularly close to the separatrix so that a variation of the level of losses with ripple amplitude is limited (see Figure 1). It means that this mechanism is unlikely to explain the observed difference in ELM frequency between “identical” JET and JT-60U ELMy H-mode.

III. ELM suppression by RMP

Unlike magnetic ripple, a stochastic magnetic field induced by external resonant magnetic perturbation (RMP) mainly increases electron transport along magnetic field lines. Recent experiment on DIII-D [4] showed that RMP could be successfully used to maintain steady-state ELM-free H-mode plasma with relatively low density. A few interesting experimental observations defy conventional transport theory logic and require further analysis and modelling. First of all, field tracing codes show that RMP should generate electron diffusion of the order of $\chi_e \sim 10 \text{m}^2/\text{sec}$ within the ETB, assuming free penetration of the RMP into DIII-D plasma [4,10]. Such a level of transport should completely destroy the edge barrier but this is not observed in the experiment. Secondly, experiment reveals that application of RMP leads to a sustained reduction of plasma density rather than that of electron temperature. Thirdly, it appears to be a power threshold below which ELMs are not fully stabilised.

Let us first discuss the level of stochastic transport generated by the RMP. It is known from theory [11] that plasma rotation can prevent an external magnetic field from penetrating through the resonant magnetic surface. This shielding reduces the width of islands on respective resonant magnetic surfaces, which in turn would prevent islands from overlapping, thus reducing the level of stochastic transport. A simple estimate of the field shielding by plasma rotation from [11] gives in a “visco-resistive” approximation:

$$B_{m,n}^{r, shielded}(r_{res}) \approx B_{m,n}^{r, vac}(r_{res}) / \sqrt{1 + \left(\frac{\Omega \cdot \tau_L}{2m}\right)^2} \equiv S_{factor} B_{m,n}^{r, vac}(r_{res}) \quad (1)$$

Here $B_{m,n}^{r, shielded}(r_{res})$ is the amplitude of the (m,n) harmonic of a shielded magnetic field at the position of the resonance $m=-nq$; $B_{m,n}^{r, vac}(r_{res})$ is the amplitude of the (m,n) harmonic of the vacuum magnetic field (unshielded) at the position of the resonance. $\Omega=2\pi m f$ is the local toroidal rotation frequency for the mode n (local means at $m=-nq$), f is the toroidal plasma rotation frequency, τ_L is a local visco-resistive layer time, defined as:

$$\tau_L \equiv 2 \cdot \left(\sqrt{1 + 2q^2} \cdot \tau_A \right)^{2/3} \cdot \frac{\tau_\eta^{2/3}}{\tau_V^{1/3}}, \text{ where } \tau_A = \frac{R}{V_A} \cdot \frac{1}{n \cdot Sh} \text{ is the Alfvén time, } V_A = \frac{B_\phi}{\sqrt{\rho \cdot \mu_0}}; n$$

is the toroidal mode number, Sh is the local magnetic shear; $A_i=2$; $Z_{eff}=1.5$; $\tau_\eta = \mu_0 \cdot r_s^2 / \eta$ is

the resistive time at the resonant magnetic surface (where $m=-nq$, $n<0$), r_s is the equivalent radius of resonant magnetic surface (here the effective ‘‘cylindrical’’ radius is taken as $r_s=a*\psi_{pol}^{1/2}$, a is the plasma minor radius ($a=0.6128$ m for DIII-D), η being the parallel plasma resistivity. The viscous time is defined as $\tau_V = \mu \cdot r_s^2$, where μ is the perpendicular ion viscosity.

Using a simple estimate for the distance between neighbouring islands: $\Delta_{m+1,m} \approx \frac{1}{nq}$, and for the island width:

$$\delta_{mn} = \sqrt{4R_0 a q^2 \left| 2B_{mn}^{r,Shielded} \right| / m \frac{dq}{ds} B_0} \quad (2)$$

one can obtain a criteria for plasma rotation, which would prevent of island overlap:

$$\delta_{mn} \geq \Delta_{m+1,m} \Rightarrow \sqrt{1 + \left(\frac{\Omega \tau_L}{2m} \right)^2} \geq 16m \cdot \frac{Sh \cdot q}{\epsilon} \cdot \frac{B_{vac}}{B_0} \quad (3)$$

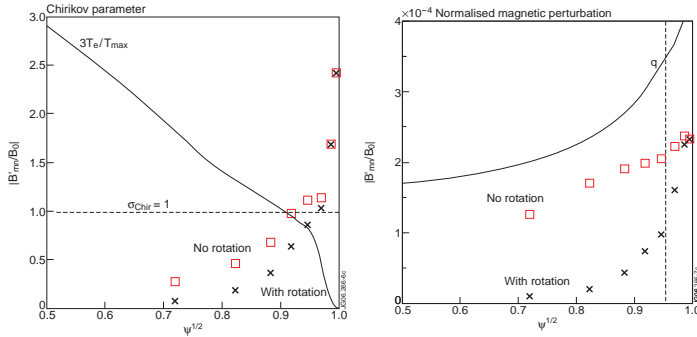


FIG. 5. Chirikov parameter with (crosses) and without (squares) rotation for the DIII-D shot #122336

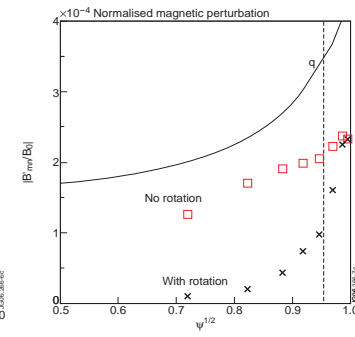


FIG. 6. Radial magnetic perturbation with (crosses) and without (squares) toroidal rotation.

Formula (3) can be used for a qualitative estimate of the effectiveness of field shielding particularly in assessing how field screening changes with plasma parameters. Formula (1) was also used in a field tracing code [11] to give a quantitative estimate of field screening by plasma rotation. The simulation was done for a typical low density DIII-D shot with RMP (#122336) with the result shown in Figures 5,6. We can conclude that

plasma rotation significantly reduces overlapping of magnetic islands in the presence of RMP, particularly inside the edge barrier.

It is worth noting that a self-consistent plasma response to the penetration of the resonant magnetic field is not taken into account in the present simulations. Generally penetration of the static RMP into rotating plasma should induce plasma braking leading to the decrease of the screening effect, resulting in a better penetration of RMP than estimated with (3). In extreme cases such a non-linear feedback can lead to the appearance of a locked mode, which would completely stop plasma rotation. This effect was recently observed in DIII-D upon application of a limited amount of counter NBI, aimed at reducing plasma rotation. Namely it was shown that even a relatively small fraction of ctr-NBI frequently caused a locked mode, which was in some cases followed by the re-appearance of ELMs or even by loss of the edge barrier altogether.

The transport code JETTO was used to simulate the dynamics of ELM suppression by RMP. The standard JETTO Bohm/gyroBohm model for anomalous transport was used in the core. A fixed width of edge transport barrier (ETB) was assumed in the simulations (with $\Delta=3$ cm) with anomalous transport within the ETB being fully suppressed so that the residual heat transport arises from the neo-classical transport and extra electron transport from the RMP, $\Delta\chi_{RMP}$. Particle diffusion comprises neo-classical plus an extra diffusivity due to intrinsically non-ambipolar electron transport. The latter can increase the overall plasma diffusion coefficient up to the level of the neo-classical ion thermal conductivity:

$$D = D_{neo-cl} + \frac{\chi_i^{neo-cl} \cdot \Delta\chi_{RMP}}{\chi_i^{neo-cl} + \Delta\chi_{RMP}} \leq \chi_i^{neo-cl} \quad (4)$$

As in section II, it was assumed that an ELM is triggered when the normalised pressure gradient exceeds a certain critical value anywhere within the ETB. We used a prescribed ELM amplitude in this simulation. The main result of the simulation for a characteristic low density DIII-D plasma is shown in Figs. 7 and 8 and allows one to conclude that qualitatively the model reproduces experimentally observed ELM suppression by RMP. It also reproduces the observed drop in plasma density when I-coils are energised. However predictive modelling

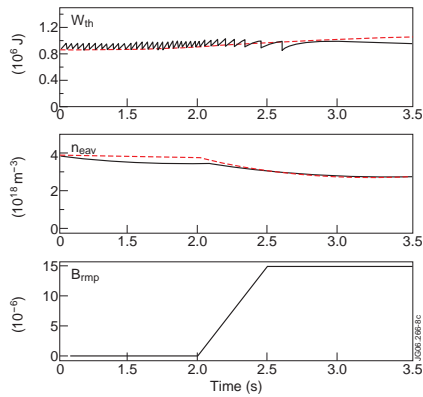


FIG. 7. Time evolution of DIII-D plasma density and energy content with RMP (red-simulation, blue-experiment) for the shot #122338

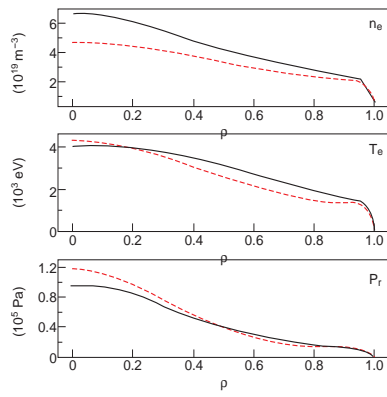


FIG. 8 Simulated (red) and measured (blue) density, temperature and pressure profiles at $t=3000ms$.

fails to reproduce some other experimentally observed trends. First of all, it can not explain why ELM suppression requires heating power above a certain threshold level. Standard transport models (with fixed transport barrier width and fixed critical pressure gradient) predict opposite trends: ELM suppression should be effective below a certain power threshold.

Secondly, modelling predicts that the ELM frequency should be reduced in the case of partial ELM stabilisation. The experimentally observed trend is often the opposite one: the ELM frequency increases and ELM amplitude drops in the case of partial stabilisation. This trend is common in plasmas with both ripple and RMP and it will be discussed in the next paragraph.

V. Role of plasma convection in pedestal behaviour and ELMs.

Experiments on JT-60U and DIII-D have at least one feature in common: particle diffusion is stronger than in “normal” ELMy H-modes, and it is not intrinsically ambipolar in both plasmas. Theory suggests that this non-ambipolarity should result in enhanced plasma convection due to appearance of an electric field leading to the formation of ExB driven convective cells near the separatrix. The result of this enhanced particle diffusion should be reduced plasma density, observed in experiment. It is also fair to say that any attempt to increase plasma density in these experiments led to a sharp increase in ELM frequency followed by degradation in plasma performance. Actually, a similar trend is observed in all tokamaks when a high level of external gas puffing is used to increase plasma density. Usually, the ELM frequency increases with the level of gas puffing and plasma performance degrades until plasma returns to a type-III ELMy H-mode or even back to L-mode. The difference between the “standard” plasmas without externally induced non-ambipolarity and the experiments discussed is that the “standard” plasma has a significantly higher level of “natural” density when the plasma has infrequent, strong type-I ELMs, as well as high energy and particle confinement. It is worth noting here that in accordance with experimental observations, strong infrequent ELMs have a large convective component in the energy losses while the energy losses during small, high frequency ELMs in high-density plasmas have a strong convective component [13].

As we discussed earlier, both magnetic ripple and RMP lead to an increased level of either ion or electron non-ambipolar transport near the separatrix. Transport modelling with the 1.5D

transport code JETTO shows that with sufficiently high amplitude of this extra transport, ELMs could be completely eliminated. A lower amplitude of additional transport should lead to partial ELM suppression, with a reduction of ELM frequency. Although experiments

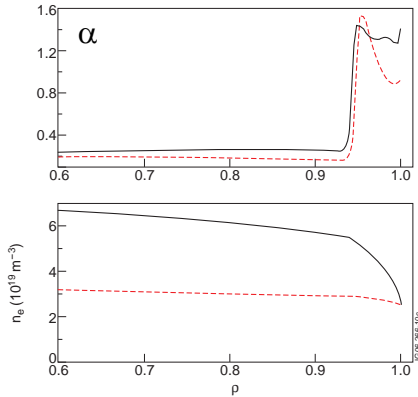


FIG.9. Radial distribution of parameter α and plasma density for plasma with low gas puffing (red) and strong gas puffing (blue)

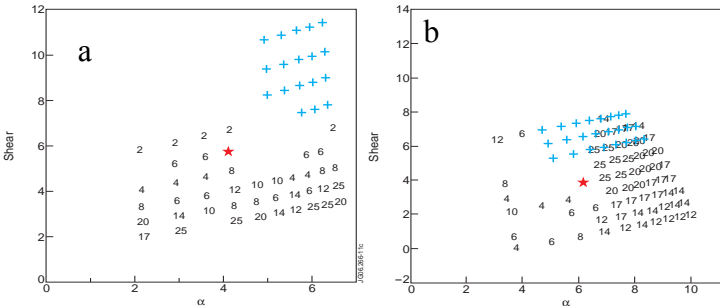


FIG. 10. MHD stability diagram for the case with pressure gradient peaked at top of barrier (a) and near the separatrix (b)

barrier is increased above the neo-classical level (or, alternatively, the level of plasma convection increases due to the high level of gas puffing), the radial distribution of pressure gradient and edge current become more monotonic or even increases towards the separatrix. We perform stability analysis of these plasmas using the MHD stability code MISHKA. This

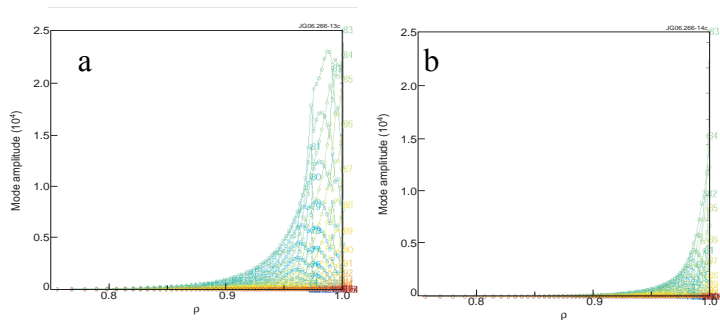


FIG. 11. Radial distribution of unstable mode for the case with pressure gradient peaked at top of barrier (a) and near the separatrix (b)

analysis reveals that MHD stability is significantly affected by the radial distribution of the edge current: plasmas with a flat distribution of pressure gradient (and edge current) having a significantly lower level of critical pressure gradient than plasma with a reduced current near the separatrix (see Fig. 10, see also [14]).

What is more, the radial distribution of the unstable modes changes from wide, centred near the top of the barrier (see Fig. 11a) for the case with a peaked pressure gradient to a very narrow one with the maximum at the separatrix in case of a uniform pressure gradient within the ETB (see Fig. 11b). This change in MHD stability threshold might have a serious implication for ELM dynamics. To

support full ELM suppression by both enhanced ripple and RMP, partial ELM suppression frequently manifests itself as an increase in ELM frequency and decrease in ELM amplitude, contrary to expectations.

To investigate the effect of enhanced plasma convection on ELM behaviour, the JETTO code was used to simulate the time evolution of plasma parameters between ELMs with different levels of particle diffusivity or gas puffing. The standard JETTO transport model described above was used. Simulations reveal two trends. First of all, as expected, with the rising level of extra transport it takes longer to reach the same level of normalised pressure gradient (parameter α) so that starting from a certain level of extra transport, the plasma never reaches peeling or ballooning instability. The second trend is less obvious. If

particle diffusivity is kept at the neo-classical level (and there is no external gas puffing), the radial distribution of the pressure gradient within the edge barrier remains highly non-uniform, with the maximum reached near the top of the pedestal (see Figs. 9, 10). The same is valid for the edge current, which is mainly generated by the bootstrap effect. If the level of transport diffusivity within the barrier is increased above the neo-classical level (or, alternatively, the level of plasma convection increases due to the high level of gas puffing), the radial distribution of pressure gradient and edge current become more monotonic or even increases towards the separatrix. This analysis reveals that MHD stability is significantly affected by the radial distribution of the edge current: plasmas with a flat distribution of pressure gradient (and edge current) having a significantly lower level of critical pressure gradient than plasma with a reduced current near the separatrix (see Fig. 10, see also [14]).

What is more, the radial distribution of the unstable modes changes from wide, centred near the top of the barrier (see Fig. 11a) for the case with a peaked pressure gradient to a very narrow one with the maximum at the separatrix in case of a uniform pressure gradient within the ETB (see Fig. 11b). This change in MHD stability threshold might have a serious implication for ELM dynamics. To

study this effect, we used a previously developed theory-motivated ELM model, in which the ELM amplitude is evaluated from the following equation for the mode displacement ξ [15]:

$$\frac{\partial \xi}{\partial t} = \sum_{j=j_{\text{topofETB}}}^{j_{\text{separatrix}}} \left[C_b \frac{c_{si}}{\sqrt{L_{pi} R_i}} \left(1 - \frac{\alpha_c}{\alpha_j} \right) H(\alpha_j - \alpha_c) \xi - C_d \frac{c_{s,j}}{R_j} (\xi - \xi_0) \right], \delta \chi \sim \xi(t) \exp \left[- \left(\frac{r - r_0}{\Delta} \right)^2 \right] \quad (5)$$

where α_{cr} is the value of normalised pressure gradient for a marginally unstable plasma, Δ being the width of the eigenfunction and r_0 is the radial localisation of its maximum.

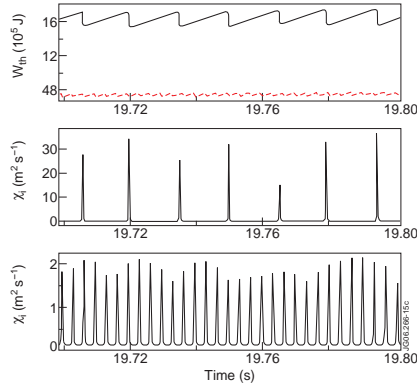


FIG. 12. Time evolution for the energy content and ELM amplitude for the case with pressure gradient peaked at top of barrier (black) and near the separatrix (red)

Equation (5) was solved alongside the transport equations in JETTO and showed that the ELM frequency increases dramatically (with confinement dropping) when plasma convection becomes strong enough to make the pressure gradient and edge current uniform within the edge barrier (see Fig. 12).

In the experiment, the two phenomena discussed in this section can partly compensate each other. Namely ELM frequency should go down when extra transport within the ETB is introduced because it takes longer to restore the pressure gradient near the edge depleted by the ELM. On other hand the ELM amplitude should drop and the ELM frequency should increase when convective losses become comparable to conductive losses between ELMs. It is therefore conceivable that the ELM frequency in the real

experiment increases with the introduction of the extra transport, with the amplitude of the ELM dropping before the ELMs were stabilised.

VI Discussion.

The results presented in this paper show that both magnetic ripple and RMP have good potential for use as a tool for ELM mitigation. Further experiments are needed, of course, to prove if these tools can be effectively used in practice. Since magnetic ripple increases ion transport and RMP electron transport, a combination of these two methods might give a very versatile tool to control both electron and ion transport in the pedestal region of the plasma.

This work was funded jointly by the United Kingdom Engineering and Physical Sciences Research Council and by the European Communities under the contract of Association between EURATOM and UKAEA. The views and opinions expressed herein do not necessarily reflect those of the European Commission. The work was also partly done under the IEA agreement on Large Tokamak Facilities.

References

- [1] G. Saibene et al., *Plasma Phys. Control. Fusion* **46** A195 (2004); G. Saibene et al., 20th IAEA Fusion Energy Conference, Vilamoura, Portugal, 2004;
- [2] B. Tubbing, *Proc. 22 EPS Conf. on Contr. Fus. Plasma Phys. Vol. 19C*, p. IV-001 (1995);
- [3] H. Urano et al., *PPCF* **48** (2006) A193;
- [4] T.E. Evans et al., *Nature Physics* **2** (2006) 419;
- [5] T. Kiviniemi et al., 33 EPS, 2005; T. Johnson et al., 34 EPS, 2006;
- [6] K. Sakurai et al., submitted to *J. Nucl. Material*, 2006;
- [7] P.N. Yushmanov, *Review of Plasma Physics*, v. 16, New York, Consultants Bureau (1991).
- [8] M. Yoshida et al., 33 EPS Conf. On Contr. Fus. Plasma Phys., Rome, 2006
- [9] J. Lonnroth et al., *PPCF* **47** 767 (2004);
- [10] M. Becoulet et al., *Nucl. Fusion*, **45**, (2005), 1284;
- [11] A. Cole and R. Fitzpatrick, *Phys. Plasmas*, **13**, 032503 (2006);
- [12] G. Saibene et al, *Proc., 28th EPS Conf. on Contr. Fus. Plasma Phys, Vol. 25A*, p 61;
- [13] Loarte A. et al 2004 *Phys. Plasmas* **11** 2668;
- [14] S. Medvedev et al. *PPCF* **48** 927 (2006);
- [15] J. Lönroth et al., *PPCF* **46** 1197 (2004).